Physica Scripta

PAPER

Thermodynamic and magnetic properties of cylindrical of nanoshell *GaAsMn* considering Rashba spin–orbit coupling

RECEIVED
17 May 2025

REVISED
8 July 2025

ACCEPTED FOR PUBLICATION
29 July 2025

PUBLISHED
8 August 2025

M Kria[1], **M El-Yadri**[2], **L M Pérez**[3], **A Tiutiunnyk**[4], **P Díaz**[5], **L Pedraja-Rejas**[3], **D Laroze**[6], **A B Davlatov**[7,*], **S C Kenfack**[8], **M Tshipa**[9] **and E Feddi**[10]

[1] Group of Optoelectronic of Semiconductors and Nanomaterials, ENSAM, Mohammed V University in Rabat, Rabat, 10100, Morocco
[2] ElectronicSystems, Sensors and Nanobiotechnologies, ENSAM, Mohammed V University in Rabat, Rabat, 10100, Morocco
[3] Departamento de Ingeniería Industrial y de Sistemas, Universidad de Tarapacá, Casilla 7D, Arica, 1000000, Chile
[4] Departamento de Física, FACI, Universidad de Tarapacá, Arica, 1000000, Chile
[5] Departamento de Ciencias Físicas, Universidad de La Frontera, Casilla 54-D, Temuco, 4780000, Chile
[6] Instituto de Alta Investigación, Universidad de Tarapacá, Casilla 7D, Arica, 1000000, Chile
[7] Namangan State University, 161 Boburshox, Namangan, 160107, Uzbekistan
[8] Laboratory of Condensed Matter-Electronics and Signal Processing (LAMACET), Department of Physics, Faculty of Science, University of Dschang, PO Box 67, Dschang, Cameroon
[9] University of Botswana, Private Bag 0022, Gaborone, Botswana
[10] School of Physics, Mohammed VI Polytechnic University, Bengurir, Morocco
[*] Author to whom any correspondence should be addressed.

E-mail: litsey111213@gmail.com

Keywords: thermodynamic, magnetic, properties, cylindrical, nanoshell

Abstract

Diluted magnetic semiconductors (DMS) continue to attract attention due to the central role of spin in their physical behavior. Among spin-related effects, Rashba spin-orbit interaction (RSO), which arises from structural inversion asymmetry and couples an electron's spin with its orbital momentum, can significantly affect thermo-magnetic properties and quantum transport. In this work, we investigate the impact of RSO on the thermodynamic and magnetic properties of GaMnAs cylindrical nanoshells by numerically solving the Schrödinger equation and deriving relevant quantities using the Boltzmann-Gibbs statistical framework. Our results reveal that RSO and external magnetic fields have antagonist effects on spin-split energy levels: the magnetic field enhances confinement by shrinking electronic orbitals, whereas RSO tends to delocalize the wavefunction, reducing confinement energy. This competition modulates the system's thermodynamic and magnetic responses. Specifically, the heat capacity shows a pronounced peak at very low temperatures, consistent with the Schottky anomaly in low-dimensional systems. Furthermore, magnetic susceptibility exhibits strong dependence on both temperature and magnetic field, and a field- and temperature-induced phase transition from ferromagnetic to paramagnetic behavior is observed.

1. Introduction

The discovery of magnetoresistance in the late 1980s marks the birth of spintronics, a field that exploits the quantum nature of electron spin alongside its charge to develop advanced electronic technologies. Since then, spintronics has enabled breakthroughs in magnetic sensing, data storage, and logic devices, leveraging spin-dependent transport phenomena for multifunctional device integration [1]. Central to spintronics is the control of spin polarization via external fields, heterostructure engineering, and spin–orbit coupling (SOC), which together provide powerful levers for modulating electronic behavior in low-dimensional systems [2–4].

Two spin-related effects should not be overlooked: Dresselhaus and Rashba effects. The Rashba and Dresselhaus effects both contribute to spin splitting in the electronic band structure, thereby influencing spin transport and quantum coherence. They describe spin-orbit interactions in low-dimensional systems lacking inversion symmetry. The Rashba and Dresselhaus spin-orbit interactions both induce spin splitting, but Rashba

arises from structural inversion asymmetry, while Dresselhaus originates from bulk inversion asymmetry. Their competition leads to anisotropic spin textures, which can be tuned to achieve spin control in nanostructures [5, 6].

In parallel, thermodynamic studies in semiconductor nanostructures have gained increasing attention, particularly for understanding electron behavior at low temperatures under magnetic fields. Quantities such as entropy, heat capacity, and magnetic susceptibility reveal subtle many-body effects and phase transitions, especially in systems with spin-polarized states. For example, De Groote *et al* [7] analyzed the heat capacity and magnetization of two electrons in a quantum dot, showing Schottky-like anomalies at low temperatures. This thermodynamic fingerprint has since been confirmed in other studies involving spin–orbit coupling [8–12]. Similarly, Gumber *et al* [13] and Boyacioglu *et al* [14] demonstrated that quantum confinement and magnetic field effects in quantum dots induce pronounced peaks in heat capacity and entropy. Nguyen and Peeters [15] further revealed field-tunable thermodynamic transitions linked to magnetic impurities and spin interactions in nanodots. In addition to earlier foundational studies, several recent works have further emphasized the role of spin-orbit interaction and magnetic field coupling in low-dimensional magnetic systems. For instance, Shi *et al* [16] examined magnetocaloric effects and spin transitions in curved CrI_3-like bilayers, revealing temperature- and field-driven magnetic switching. Similar Schottky-like anomalies in heat capacity and entropy were observed in Kagome and decorated square nanostructures, where spin configuration and lattice geometry interplay to determine thermal responses [17, 18].

Recent literature also emphasizes the importance of geometry in shaping quantum and thermodynamic behavior. Cylindrical nanoshells, in particular, offer a compelling model system due to their quasi-one-dimensional confinement, radial symmetry, and compatibility with experimental fabrication methods. The Rashba effect in such curved geometries induces nontrivial spin splitting and modifies the spatial distribution of electronic states. El-Yadri *et al* [19] showed that magnetic field confinement in core–shell GaAs nanowires strongly affects electron localization and threshold core radii. In our previous work [20], we found that temperature, shell thickness, and quantum size dictate the behavior of the heat capacity in cylindrical quantum dots, including Schottky anomalies and thermodynamic instability. These findings motivate our focus on cylindrical GaMnAs nanoshells, where spin–orbit coupling, magnetic field, and geometry act in concert to shape physical properties.

In this paper, we investigate the thermodynamic and magnetic properties of *GaAsMn* nanoshell considering RSO coupling. The study is organized as follows: section 2 presents the background theory and its development. In section 3, we present the details of the numerical results and discussions. Finally, the conclusion is outlined in the section 4.

2. Background theory

The progress achieved in nano technology allows one to fabricate a highly ordered array of long nanoshell, such that each nanoshell is characterized by an inside and outside diameters with few monolayers for the thick. Under this assumption, let us consider an electron confined in a $Ga_{1-x}Mn_xAs$ cylindrical nanoshell defined by an outer (R_s) and an inner (R_c) radii as shown in figure 1. These cylindrical nanoshells are typically enclosed by a dielectric material with a wide band gap. This dielectric environment confines charge carriers inside the shell, which behaves as a potential well defined by its thickness ($L_w = R_s - R_c$).

Let us determine the energy of an electron confined in cylindrical nano wire when a uniform magnetic field is applied, ($\mathbf{B} = B\hat{\mathbf{k}}$) described by a vector potential in the Lorentz gauge's, $\mathbf{A} = (\mathbf{B} \times \mathbf{r})/2$. Taking into account the Rashba spin-orbit and the Zeeman interaction, the Hamiltonian of the system can be written as:

$$\mathcal{H} = \mathcal{H}_0 + \mathcal{H}_R^{SO} + \mathcal{H}_z, \tag{1}$$

where $\mathcal{H}_0$ being the Hamiltonian without considering the Rashba spin orbit effect, which can be cast in form

$$\mathcal{H}_0 = \frac{1}{2m_e^*}\left(\mathbf{p} + \frac{e\mathbf{A}}{c}\right)^2 + V_w(\rho), \tag{2}$$

where e stands for the electron charge, m_e^* is the effective mass of the electron, and $\mathbf{p}$ is the momentum of the electron. As per our supposition, the confining potential energy, $V_w(\boldsymbol{\rho})$, is provided by:

$$V_w(\boldsymbol{\rho}) = \begin{cases} 0 & R_s < \rho < R_c \\ \infty & \rho < R_s \text{ and } \rho > R_c \end{cases} \tag{3}$$

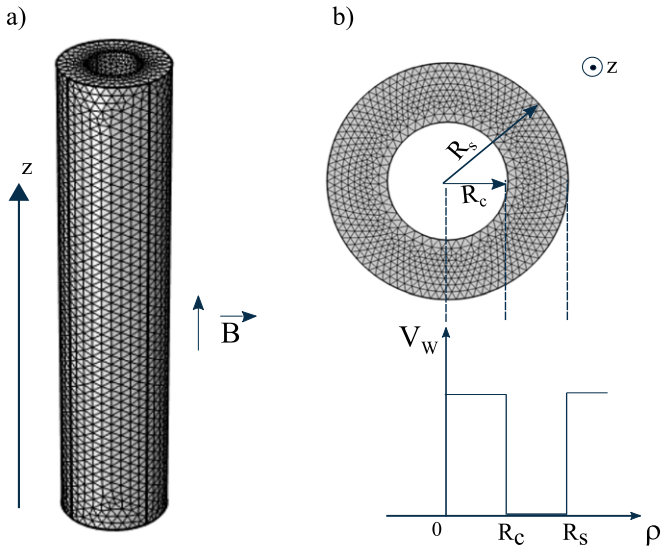

Figure 1. (a) 3D view of a cylindrical nano-shell represented with a mesh visualization, showing the structural geometry under a uniform magnetic field applied along the cylinder axis. (b) Top view of the cylindrical nano-shell with the inner radius R_c and outer radius R_s illustrating the radial confinement potential.

The Rashba spin-orbit Hamiltonian is denoted by the second term $\mathcal{H}_R^{SO}$, which is written as follows [21]:

$$\mathcal{H}_R^{SO} = \frac{\alpha_R}{\hbar}\left[\hat{\sigma} \quad \times \left(\mathbf{p} + \frac{e\mathbf{A}}{c}\right)\right], \tag{4}$$

where α_R represents the Rashba coupling parameter, c stands for the velocity of electromagnetic waves in vacuum and $\hat{\sigma}$ the well-known Pauli spin matrices with $\sigma_x = \begin{pmatrix} 0 & 1 \\ 1 & 0 \end{pmatrix}$, $\sigma_y = \begin{pmatrix} 0 & -i \\ i & 0 \end{pmatrix}$, $\sigma_z = \begin{pmatrix} 1 & 0 \\ 0 & -1 \end{pmatrix}$. The third term in equation (1) represents the Zeeman interaction:

$$\mathcal{H}_Z = \frac{1}{2} g^* \mu_B B \sigma_z, \tag{5}$$

such that g^* is the Lande's factor of the electron and $\mu_B = \frac{e\hbar}{2m_0 c}$ is the Bohr magneton.

By solving the Schrödinger equation, $\mathcal{H}\Psi(\rho, \varphi) = E\Psi(\rho, \varphi)$, one can determine the system's fundamental and excited energies as well as its wave functions. Taking into account the spin states, the Hamiltonian of the system given in equation (1) can be writen as a 2×2 matrix. Therefore, the Schrödinger equation can be expressed as:

$$\begin{pmatrix} \mathcal{H}_{11} & \mathcal{H}_{12} \\ \mathcal{H}_{21} & \mathcal{H}_{22} \end{pmatrix} \begin{pmatrix} \Psi_+ \\ \Psi_- \end{pmatrix} = E \begin{pmatrix} \Psi_+ \\ \Psi_- \end{pmatrix} \tag{6}$$

where $\Psi_+ = \begin{pmatrix} 1 \\ 0 \end{pmatrix}\Psi_\uparrow$ and $\Psi_- = \begin{pmatrix} 0 \\ 1 \end{pmatrix}\Psi_\downarrow$ are the spinor wave functions with spin up and down eigenfuctions of σ_z. The different expressions of the operators $\mathcal{H}_{ij}$ can be written as:

$$\mathcal{H}_{11} = \frac{-\hbar^2}{2m_e^*}\left(\frac{\partial^2}{\partial x^2} + \frac{\partial^2}{\partial y^2} + \frac{\partial^2}{\partial z^2}\right) + \frac{e^2B^2}{8m_e^* c^2}(x^2 + y^2) + \frac{ieB\hbar}{2m_e^* c}\left(x\frac{\partial}{\partial y} - y\frac{\partial}{\partial x}\right) + \frac{1}{2}g^*\mu_B B + V_w(x, y), \tag{7}$$

$$\mathcal{H}_{22} = \frac{-\hbar^2}{2m_e^*}\left(\frac{\partial^2}{\partial x^2} + \frac{\partial^2}{\partial y^2} + \frac{\partial^2}{\partial z^2}\right) + \frac{e^2B^2}{8m_e^* c^2}(x^2 + y^2) + \frac{ieB\hbar}{2m_e^* c}\left(x\frac{\partial}{\partial y} - y\frac{\partial}{\partial x}\right) - \frac{1}{2}g^*\mu_B B + V_w(x, y), \tag{8}$$

$$\mathcal{H}_{12} = \alpha_R\left(\frac{\partial}{\partial x} - i\frac{\partial}{\partial y} - \frac{eB}{2\hbar c}(x + iy)\right) \tag{9}$$

and

$$\mathcal{H}_{21} = -\alpha_R\left(\frac{\partial}{\partial x} + i\frac{\partial}{\partial y} + \frac{eB}{2\hbar c}(-x + iy)\right). \tag{10}$$

If we take into account the relationship $x = \rho\cos\varphi$, $y = \rho\sin\varphi$ and $\rho = \sqrt{x^2 + y^2}$ between the Cartesian and cylindrical coordinate systems, the $\mathcal{H}_{ij}$ Hamiltonian operators take the following form:

$$H_{11} = -\frac{\hbar^2}{2m^*}\left[\frac{\partial^2}{\partial\rho^2} + \frac{1}{\rho}\frac{\partial}{\partial\rho} - \frac{1}{\rho^2}\left(i\frac{\partial}{\partial\varphi} - \frac{Be\rho^2}{2\hbar}\right)^2\right] + \frac{1}{2}g^*B\mu_B + V_w(\rho) \tag{11}$$

$$H_{22} = -\frac{\hbar^2}{2m^*}\left[\frac{\partial^2}{\partial\rho^2} + \frac{1}{\rho}\frac{\partial}{\partial\rho} - \frac{1}{\rho^2}\left(i\frac{\partial}{\partial\varphi} - \frac{Be\rho^2}{2\hbar}\right)^2\right] - \frac{1}{2}g^*B\mu_B + V_w(\rho) \tag{12}$$

$$H_{12} = \alpha_R e^{-i\varphi}\left[\frac{\partial}{\partial\rho} - \frac{i}{\rho}\frac{\partial}{\partial\varphi} + \frac{Be\rho}{2\hbar}\right] \tag{13}$$

$$H_{21} = \alpha_R e^{i\varphi}\left[-\frac{\partial}{\partial\rho} - \frac{i}{\rho}\frac{\partial}{\partial\varphi} + \frac{Be\rho}{2\hbar}\right] \tag{14}$$

The eigenfunctions of H can be split as the sum of two spin-polarized spatial wave functions,

$$\Psi = \Psi_\uparrow + \Psi_\downarrow \tag{15}$$

where :

$$\Psi_\uparrow = \frac{1}{\sqrt{2\pi}}\sum_{n,l} a_{n,l,\uparrow}e^{il\varphi}\Phi_{nl}(\rho) \tag{16}$$

and

$$\Psi_\downarrow = \frac{1}{\sqrt{2\pi}}\sum_{n,l} a_{n,l,\downarrow}e^{il\varphi}\Phi_{nl}(\rho) \tag{17}$$

are the totally polarized spatial wave functions with spin-up and spin-down, respectively.

Equation (6) was implemented and solved using the Finite Element Method (FEM) through the Partial Differential equation (PDE) module in COMSOL Multiphysics [22]. To ensure accurate modeling of the confinement, Neumann ($\hat{n}\cdot\nabla\psi = 0$) and Dirichlet ($\psi = 0$) boundary conditions were applied at the inner and outer surfaces of the shell. These boundary conditions effectively encapsulated the quantum system, allowing for precise simulation of the electron's behavior and its interactions within the nanoscale structure. An extra-fine computational mesh and appropriate normalization constraints were employed to ensure numerical stability and physical relevance of the solutions.

Once obtained, the eigenenergies can then be used to investigate the thermodynamic properties. According to the Boltzmann-Gibbs statistics, the total number of microstates in confined system is defined by the distribution of particles over energy levels. The number of quantum energy states labeled by the index i is finite, and can be used to determine the canonical partition function Z_c which will be used to calculate fundamental thermodynamic and magnetic properties within the context of the Boltzmann-Gibbs statistics. It is given from the sum over all energy levels E_i as follows [23]:

$$Z_c = \sum_i \exp\left(-\beta(E_i^+ + E_i^-)\right), \tag{18}$$

where $\beta = 1/(k_BT)$ is the inverse product of the temperature and the Boltzmann constant, k_B. The partition function Z_c allows the deduction of the system's primary thermodynamic characteristics. It is related to the mean energy of the system by the relation:

$$\langle E\rangle = -\frac{\partial\ln Z_c}{\partial\beta}. \tag{19}$$

The thermodynamic potential: Ω can be deduced from the partition coefficient via the relation:

$$\Omega = k_B\ln Z_c \tag{20}$$

We recall that for an ideal electron gas in semiconductor nanowires it has the following form [24]

$$\Omega = -k_BT\frac{1}{\pi}\sqrt{\frac{2m^*}{\hbar^2}}\sum_i\int_{E_i}^{\infty}\ln\left(1 + \exp\left(\frac{\mu - E}{k_BT}\right)\right)\frac{1}{\sqrt{E - E_i}}dE \tag{21}$$

Moreover, entropy is one of the most significant thermodynamic characteristics that controls randomness in the system. The most popular entropy is the Shannon entropy [25]. By using Tsallis approach given in the frame work of Boltzmann-Gibbs statistical mechanics [26], the entropy of an electron gas in semiconductor nanowires is given by:

$$S = -\frac{\partial \Omega}{\partial T} \tag{22}$$

which leads to the analytical expression:

$$S = \frac{k_B}{\pi}\sqrt{\frac{2m^*}{\hbar^2}}\sum_i \int_{E_i}^{\infty}\left(\ln\left(1+\exp\left(\frac{\mu - E}{k_B T}\right)\right) - \frac{\frac{\mu - E}{k_B T}}{1+\exp\left(\frac{E-\mu}{k_B T}\right)}\right)\frac{1}{\sqrt{E-E_i}}dE \tag{23}$$

Consequently, one can compute the heat capacity, which defines the quality of the stored energy [24] as

$$C_v = -T\frac{\partial^2 \Omega}{\partial T^2} = T\frac{\partial S}{\partial T} \tag{24}$$

$$C_v = \frac{k_B}{\pi}\sqrt{\frac{2m^*}{\hbar^2}}\sum_i \int_{E_i}^{\infty}\frac{\left(\frac{E-\mu}{2k_B T}\right)^2}{\cosh^2\left(\frac{E-\mu}{2k_B T}\right)}\frac{1}{\sqrt{E-E_i}}dE. \tag{25}$$

The Helmholtz free energy, given by the relation $F_H = -\frac{\ln \Omega}{\beta}$, where ($\beta = 1/(k_B T)$), provides the stability requirement. It is also related to the the entropy by the relation: $S = -\left(\frac{\partial F}{\partial T}\right)_V$.

The magnetic behavior of the system can be investigated through its magnetization when exposed to a magnetic source. This property is identified by the magnetic susceptibility $\chi = \partial M/\partial B$. Magnetization M (magnetic moment per unit volume) can be obtained by the relation:

$$M = -\frac{\partial \Omega_L}{\partial B}. \tag{26}$$

It is important to note that the sign of the susceptibility χ indicates the magnetic behaviors. In particular, $\chi < 0$ denotes paramagnetism, while diamagnetism appears when $\chi > 0$.

3. Numerical results and discussion

Our model is applied to $Ga_{1-x}Mn_xAs$ nanoshell. The physical parameters used in this study are as follows. We apply our model to $Ga_{1-x}Mn_xAs$ nanotubes corresponding to a hollow cylinders [27]. The physical parameters used here are as follows: $m_e^* = 0.067 m_0$, $g^* = 2$, $\varepsilon(x = 0.03) = 11.8$ and $E_g(x = 0.03) = 1.5\ eV$ [28].

In our previous work [29], we have demonstrated and discussed in detail the fact that optoelectronic properties depend strongly on thickness of the shell $L_w = R_s - R_c$. Therefore, in this study, we restrict ourselves to the limit of strong confinement regime corresponding $L_w = 10\ nm$ with an outer radius $R_s = 40\ nm$, an inner radius $R_c = 30\ nm$, and a height $H = 100\ nm$.

To understand the causality between RSO and magnetic field effects, we begin by emphasizing the fact that the existence of *Mn* ions induces an internal electric local polarization inside elementary structures due to high polarizability inside the elementary cell. This spontaneous polarization breaks the system's symmetry, leading to an enhancement of spin–orbit coupling, specifically the Rashba effect, where an electron's spin becomes strongly coupled to its momentum. However, a magnetic field is not fundamentally necessary to trigger the Rashba effect, but rather it intervenes to orient the spins and split the electronic states. To better understand this relation, we examine how charge distribution evolves under the combined influence of intrinsic polarization and an external magnetic field. Indeed, the behavior of charge densities under the influence of a magnetic field and the Rashba effect can be analyzed separately and jointly since the both interactions influence electrons in opposite ways. To illustrate these antagonistic effects, we plot in figures 2(a), (b) the *xy*-plane projection of the spatial distribution of spin up (spin down) by combining magnetic field (B) and RSO effects described by the parameter (α_R). We choose (B= 0, 1 and 2T) for magnetic field and ($\alpha_R = 0$, 2 and $4 \times 10^{-11} eV.m$) for RSO coupling coefficient. As we can remark, the spin-down electron probability density dominates when $\alpha_R = 0$ and $B = 0$. This can be attributed to the intrinsic exchange interaction in $Ga_{1-x}Mn_xAs$. This dilute magnetic semiconductor contains localized magnetic moments associated with the *Mn* atoms, which interact with the spins of conduction electrons. The exchange coupling between these localized moments and the electron spins breaks the spin degeneracy, effectively lowering the energy of the spin-down states relative to the spin-up states. As a result, electrons preferentially occupy randomly the spin-down states, leading to a higher probability density for this

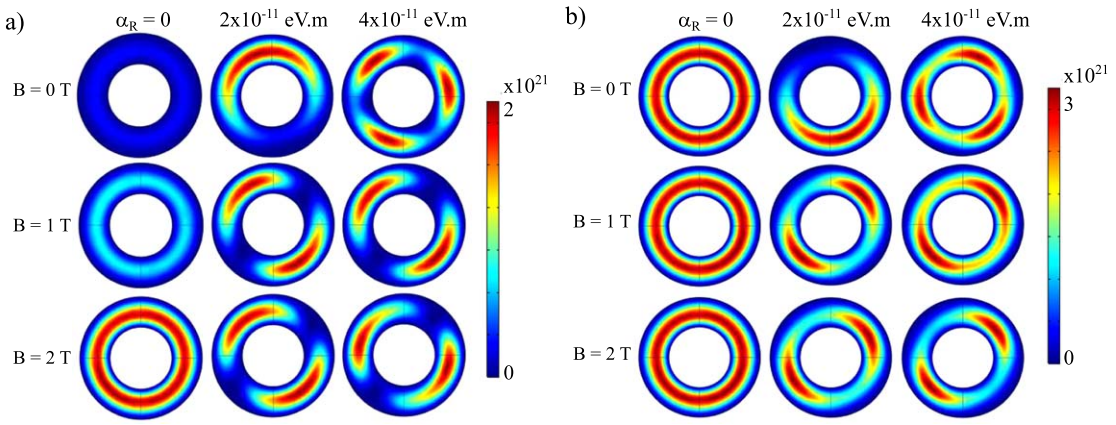

Figure 2. Cross-sectional view (*xy*-plane) of the spatial electron densities with spin up (a) and spin down (b). In each matrix, we cross 3 values of magnetic field B= (0, 1, and 2T) and 3 values of RSO coupling $\alpha_R = 0, 2,$ and $4 \times 10^{-11} eV.m$.

spin orientation. The first line in figure 2, clearly shows that the RSO can exist even at a zero magnetic field ($B = 0$) as mentioned above. We note that by increasing the RSO coefficient, the Rashba coupling causes an energy splitting of electronic states based on their spin, leading to changes in charge densities. Indeed, due to intrinsic electric field, the charge densities can be distributed asymmetrically in real space resulting in spatial charge polarization. The observed asymmetry in the electron probability density suggests that the Rashba effect alters the spin orientation across the nanoshell.

Let us analyse the magnetic field effect: As shown in 2nd and third line in figures 2(a) and (b), the spin-up electron probability density becomes increasingly pronounced with an increase in the magnetic field strength. This quantization leads to concentric rings of charge density in real space. The magnetic field further influences spin populations, leading to the opposite spin polarization compared to the direction of the applied magnetic field. The simultaneous effects of the RSO and magnetic field can lead to intricate phenomena, such as the formation of helical surface states. In these states, charge densities are modulated by both spin and Landau levels. The combination between these effects introduces spin dependence into the band structure's anisotropy, resulting in new configurations of charge densities that reflect both spin and momentum dynamics.

Given that all thermodynamic functions depend on average energy, it seems necessary to analyze the behavior of this important parameter with respect to the magnetic and RSO effects. Thus, after computing the partition function Z_c by summing over all possible states, we proceed to the determination of the mean energy given by the relation equation (19).

Our results are summarized in figures 3 and 4. We plot the the ten lowest energy levels for both spin up (solid line) and spin down (dashed line) states, considering variations in magnetic field and Rashba spin–orbit coupling. Figure 3 shows how the energy levels respond to increasing Rashba coupling $\alpha_R = 4, 5,$ and $6 \times 10^{-11} eV.m$, with the magnetic field held constant. As α_R increases, both spin-up and spin-down energy levels decrease, and the splitting between them becomes more pronounced. This indicates that strong Rashba interaction reduces the overall confinement and magnetic energy by delocalizing the electronic wavefunctions.

To further quantify the interplay between Rashba and magnetic effects, figure 4 presents the energy levels at three values of magnetic field $B = 1, 1.5$ and $2T$, for a fixed Rashba parameter $\alpha_R = 6 \times 10^{-11} eV.m$. These plots demonstrate how increasing the magnetic field enhances spin splitting and energy level shifting due to magnetic confinement, counteracting the delocalizing influence of the Rashba interaction.

Figure 5(a) illustrates the variation of heat capacity with temperature for three values of the Rashba parameter ($\alpha_R = 4, 5,$ and 6×10^{-11} eV · m) at fixed magnetic field $B = 0.5$T. Figure 5(b) presents the corresponding variation for magnetic fields $B = 1, 1.5,$ and 2T at fixed $\alpha_R = 5 \times 10^{-11}$ eV · m. In both cases, the heat capacity displays a two-peak structure. The first sharp peak at low temperatures corresponds to a Schottky anomaly, typically arising from thermal activation between two spin-split energy levels. As temperature increases, this peak broadens and shifts due to increased Rashba coupling or stronger magnetic fields, both of which reshape the energy spectrum. The second, broader peak at higher temperatures stems from the progressive population of higher-lying excited states, where the interplay between Rashba delocalization and magnetic confinement governs level density and energy spacing. The Rashba effect tends to reduce confinement and increase level mixing, while the magnetic field compresses the electronic states. This competition creates a non-monotonic density of states, which results in enhanced specific heat absorption at intermediate temperatures. As temperature further increases, level populations become saturated, leading to a decline in heat capacity.

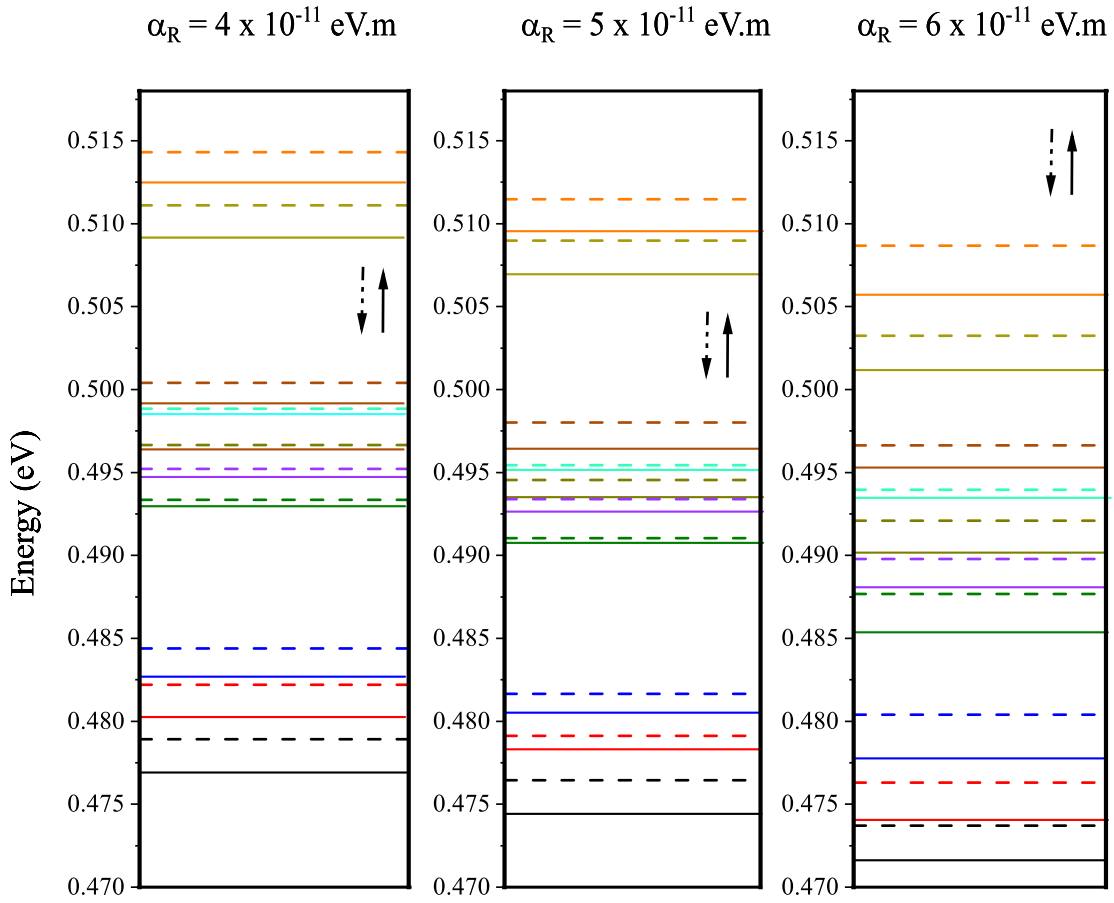

Figure 3. The ten lowest energy levels for spin-up (solid lines) and spin-down (dashed lines) states in a $Ga_{1-x}Mn_xAs$ cylindrical nanoshell are shown for Rashba parameters $\alpha_R = 4, 5$ and $6 \times 10^{-11} eV.m$ at a magnetic field of $B = 1T$.

To make clear the dependence of the heat capacity on both external parameters B and T, we present in figure 6 the contour plot of this thermodynamic parameter. We can clearly see that, in the region 1.3 to 2 T for magnetic field and 75 to 200 K for temperature, the NQDS system stores considerably the energy. The contour plot in figure 6 illustrates the dependence of the heat capacity on both the magnetic field (B) and the temperature (T) in the cylindrical *GaMnAs* nanoshell system. A significant increase in heat capacity is observed within the range of $B \approx 1.3 - 2$ T and $T \approx 75 - 200$ K, indicating that the system efficiently stores energy in this region. This behavior can be attributed to the interplay between thermal excitations, spin–orbit coupling, and the applied magnetic field. At these temperatures, a higher population of excited states contributes to an increase in heat capacity, while the magnetic field influences the electronic structure, modifying the density of accessible energy states. The Rashba spin-orbit interaction, combined with the magnetic field effect, likely plays a key role in enhancing spin-dependent energy levels, thereby affecting the thermodynamic response. Additionally, quantum confinement effects due to the cylindrical geometry may further alter the energy spectrum, leading to the observed variations. This result suggests that the system's ability to store thermal energy is maximized in this specific range of B and T, making it a critical region for understanding the thermodynamic properties of the GaMnAs nanoshell.

Figures 7(a) and (b) display, respectively, the variation of entropy with temperature for the same sets of previous values of the spin–orbit coupling constant α_R and the magnetic field B. We can see that the entropy increases with temperature while it decreases with magnetic field. The other observation here is that the entropy is not sensitive to the RSO interaction. In the presence of the spin-orbit interaction, an ordered state or region exists for any given temperature. The most stable states of this system correlate with low values of entropy, which are produced by high magnetic field values. At low temperatures, the system is highly sensitive to the magnetic field due to Zeeman splitting, which leads to a significant separation between spin sublevels. This results in a reduced number of accessible microstates, thereby lowering the entropy as the magnetic field increases. In this regime, the magnetic field strongly polarizes the spin states, aligning them preferentially and thus decreasing the degree of disorder in the system. In contrast, at high temperatures, thermal agitation dominates and overcomes the magnetic ordering effect induced by the external field. The thermal energy k_BT becomes much larger than the Zeeman energy, allowing a larger number of microstates to be thermally accessible regardless of the magnetic

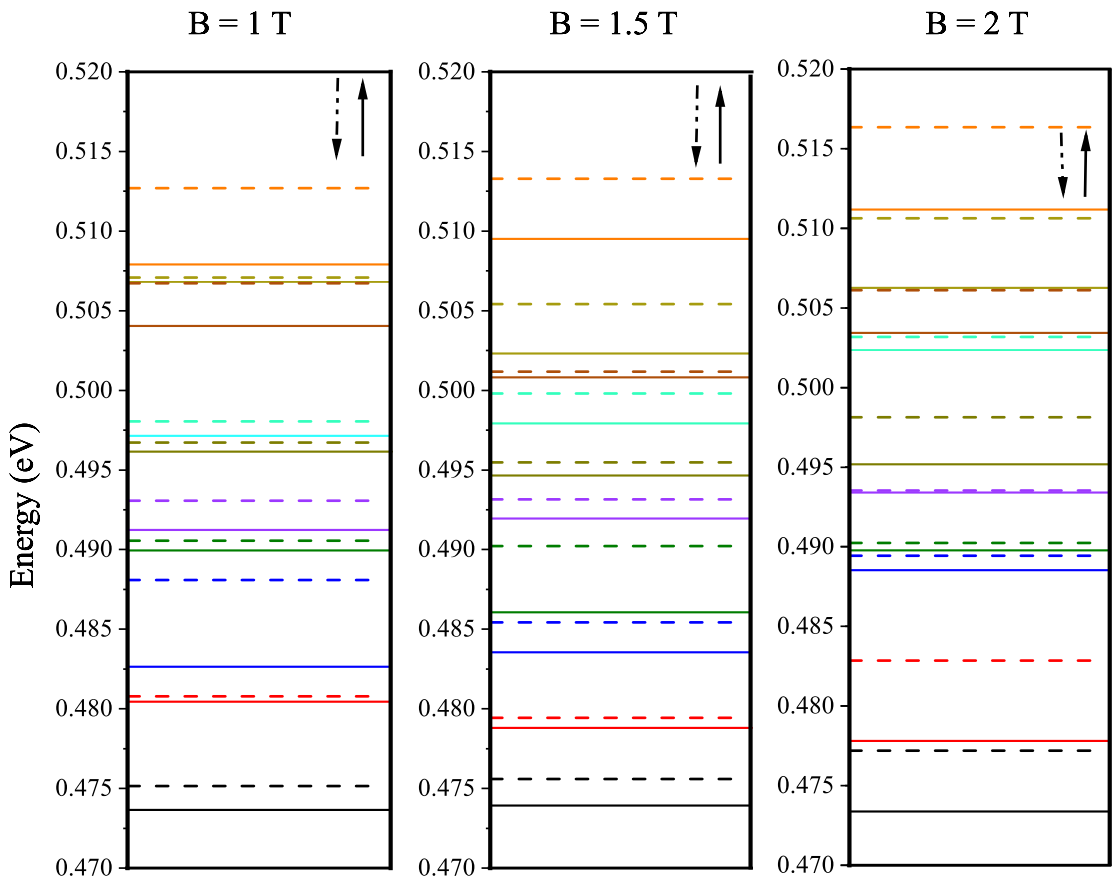

Figure 4. The ten lowest energy states for spin-up (solid arrow) and spin-down (dashed arrow) in a $Ga_{1-x}Mn_xAs$ cylindrical nanoshell are presented for three magnetic field values $B = 1, 1.5$ and $2T$ with a fixed Rashba parameter of $\alpha_R = 5 \times 10^{-11} eV.\, m$.

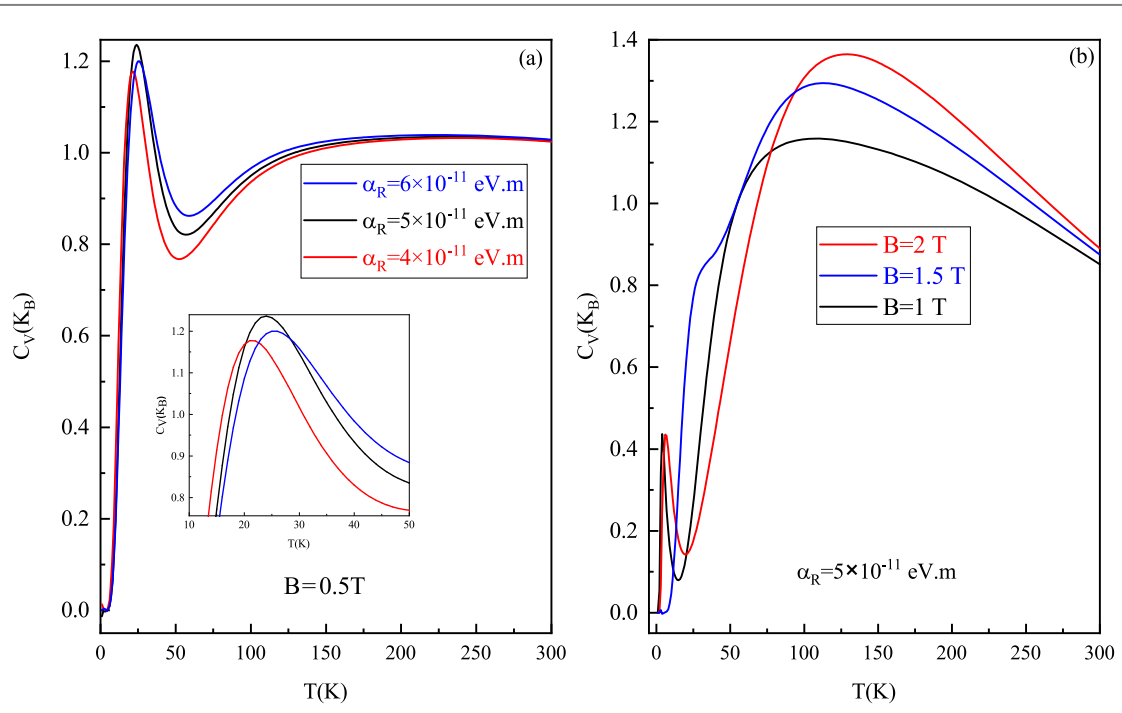

Figure 5. Heat capacity versus temperature. (a) For three values Rashba parameters $\alpha_R = 4, 5$ and $6 \times 10^{-11} eV.\, m$ at fixed magnetic field $B = 0.5\ T$. (b) For three values of the magnetic field $B = 1, 1.5$ and $2\ T$ at fixed Rashba parameter $\alpha_R = 5 \times 10^{-11} eV.\, m$.

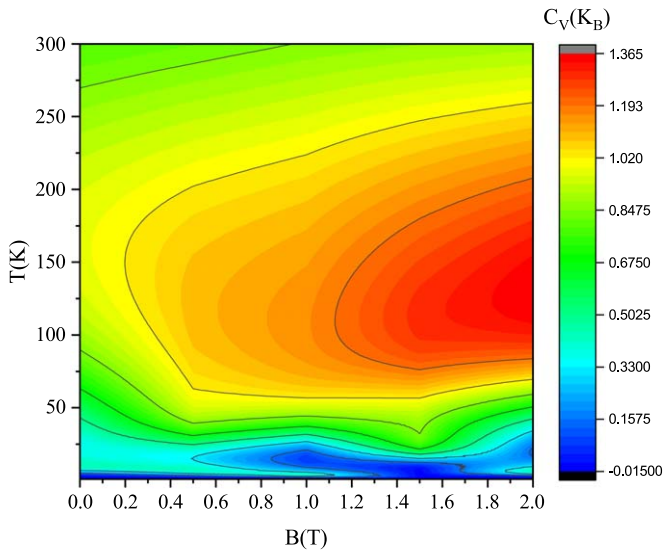

Figure 6. Heat capacity contour diagram of the temperature and magnetic field.

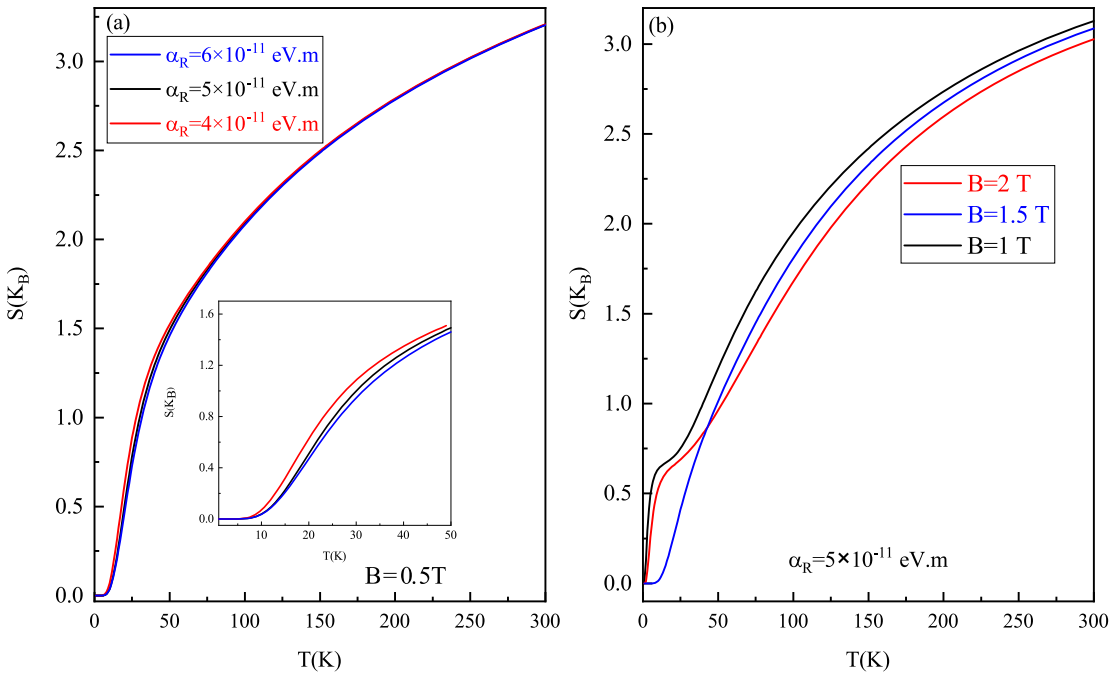

Figure 7. Entropy versus temperature. (a) For three values Rashba parameters $\alpha_R = 4, 5$ and $6 \times 10^{-11} eV.m$ at fixed magnetic field $B = 0.5\ T$. (b) For three values of the magnetic field $B = 1$, 1.5 and 2 T at fixed Rashba parameter $\alpha_R = 5 \times 10^{-11} eV.m$.

field strength. Consequently, the entropy increases with temperature in all cases, and the differences between the curves corresponding to different magnetic fields diminish. In this regime, the entropy is mainly governed by thermal excitations, and the influence of the magnetic field becomes less significant. The most reachable ordered states are understood to lie between these potential states and are located by the presence of these minimal entropy values, along with the α_R function under temperature and an external magnetic field. Thus, one can modify the α_R value and the external magnetic field in order to control the entropy in a quantum system.

To study the thermodynamic stability of our structure, we display in figure 8 the Helmholtz free energy F_H versus temperature for three different values of the Rashba parameters (a) and the magnetic field (b). The stability criterion indicates that a system is stable if it has a low Helmholtz energy (F). The results indicate that F_H decreases as temperature and the Rashba spin–orbit coupling of the system increase (figure 8(a)), while it

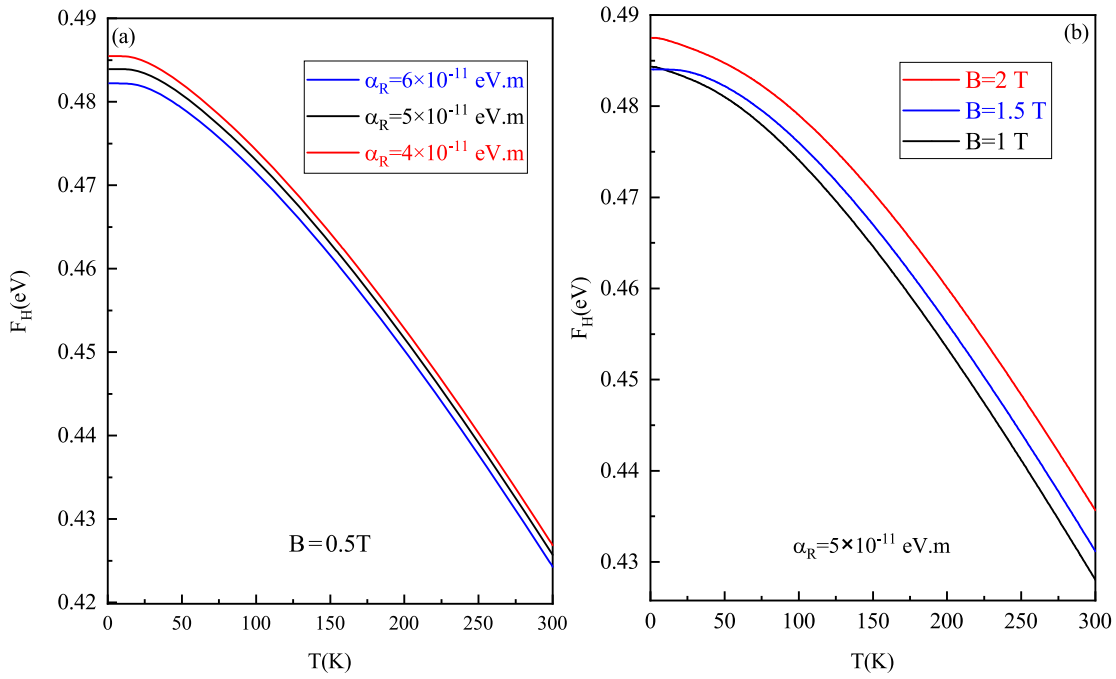

Figure 8. Helmholtz free energy versus temperature. (a) For three values of the Rashba parameter $\alpha_R = 4, 5$ and $6 \times 10^{-11} eV.m$ at fixed magnetic field $B = 0.5\ T$. (b) For three values of the magnetic field $B = 1, 1.5$ and $2\ T$ at fixed Rashba parameter $\alpha_R = 5 \times 10^{-11} eV.m$.

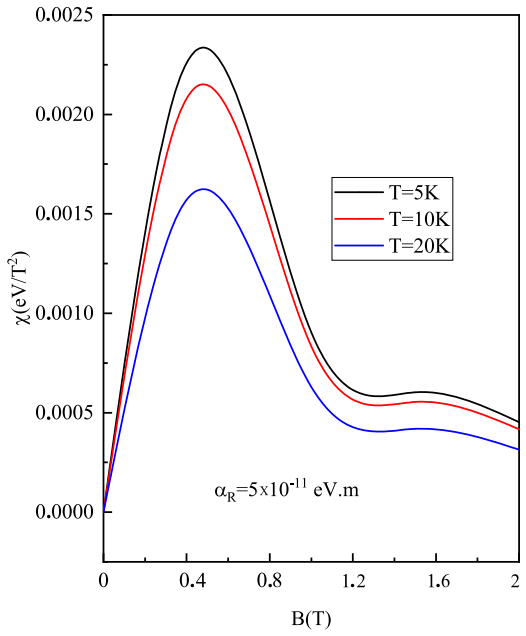

Figure 9. Magnetic susceptibility versus magnetic filed for three values of temperature $T = 5, 10$ and $20\ K$ and $\alpha_R = 5 \times 10^{-11} eV.m$.

increases with increasing magnetic field (figure 8(b)), since the magnetic field acts as an additive confinement that shrinks electronic orbitals.

Figure 9 depicts the variation of magnetic susceptibility of the nanoshell with the magnetic field strength for three low values of temperature $T = 5, 10$ and $20\ K$ with a fixed Rashba coupling $\alpha_R = 5 \times 10^{-11} eV.m$. The magnetic susceptibility increases with increasing magnetic field strength and maxima at a magnetic field that ranges between 0.5 and 0.6 T regardless of the value of temperature. As can be seen from the graph, at these low temperatures, an increase in the temperature decreases the magnetic susceptibility.

The dependence of magnetization on the magnetic field is shown in figure 10 for three low values of temperature $T = 5, 10$ and $20\ K$ and for a given $\alpha_R = 5 \times 10^{-11} eV.m$. The magnetization curves reach their

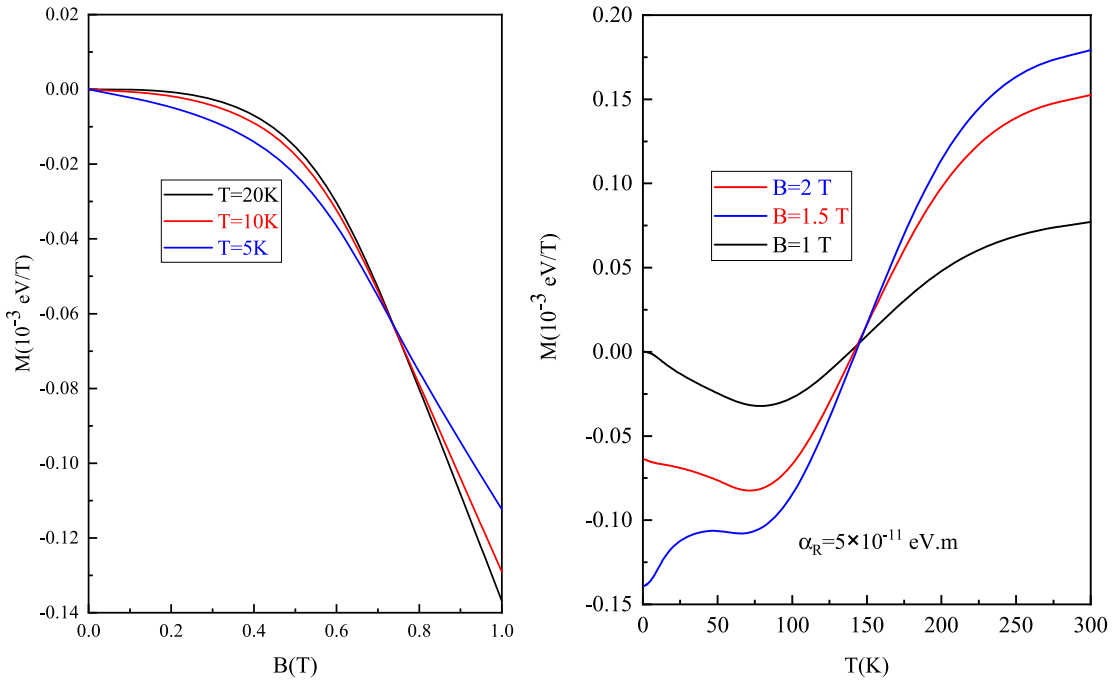

Figure 10. Magnetization versus temperature for three values of magnetic filed $B = 1$, 1.5 and 2 T and $\alpha_R = 5 \times 10^{-11} eV.m$.

maxima at magnetic field ranging between 0.5 and 0.6 T regardless of the value of temperature. The curves of the magnetization show that a slight increase in temperature leads to a decrease in magnetization and also to a small shift of the maximum towards higher values of the magnetic field. This is caused by the magnetic moment of the particle whose origin leading to the magnetization can be both electric microscopic currents, which result from the movement of the electron spin. In fact, net magnetization is generated by the reaction of a material to an external magnetic field. Increasing temperature distinguishes. Paramagnetic materials exhibit a weak, field-induced magnetization that disappears once the external magnetic field is removed. In a magnetic field, ferrimagnetic and ferromagnetic media are more strongly magnetized, and can even be magnetized without an external field, thus forming a stable magnetic. The types of the materials are highlighted when we consider this system.

Figure 9 shows a graph of magnetic susceptibility of the cylindrical nanoshell as a function of the applied magnetic field at three fixed temperature values: $T = 5$, 10 and 20 K. Figure 10 illustrates how magnetic susceptibility reflects the behavior of magnetization under varying field strengths. Magnetic susceptibility is a simple way to measure magnetization of a material in an applied magnetic field. We can conclude that our approach provides a straightforward classification of the majority of material reactions to an applied magnetic field: an orientation to the magnetic field, $\chi > 0$, known as paramagnetism. The paramagnetic materials align with the applied magnetic field and are drawn to regions of higher intensity. Due to the same considerations as outlined above, at the minimum temperature and the lowest magnetic field, the system is found to be in the paramagnetic domain. The susceptibility and the rate of change of magnetization are well known, figure 9 confirms the results of figure 10 which shows a paramagnetic magnetic phase. This magnetic property is therefore extremely dependent on temperature and magnetic field. The present work allows the classification of the phase transition that can be obtained by treating the spin–orbit coupling. The latter can be used to build quantum memories and computers, which considerably increases the efficiency of electronic devices. Our predictions agree with many existing theoretical and experimental works [13, 30, 31].

Finally, we discuss the behavior of magnetization, which, in general, refers to how a material reacts to an applied magnetic field and how the material changes under the influence of a magnetic field. The paramagnetic materials exist when the magnetization is negative, and ferrimagnetic character exist for high values of magnetization. As we can see in figure 10, the influence of magnetic field and temperature on magnetization has been analyzed. In particular, it can be seen that at low temperatures, the magnetic field lowers the magnetization, while for high temperatures, the opposite situation occurs and the magnetic field reinforces the magnetization. This situation occurs after the critical temperature $T = 150$ K for which the magnetization is independent on the magnetic field and is approximately zero. This result also shows that by modifying the magnetic characteristics of a $Ga_{1-x}Mn_xAs$ nanoshell, the system can be changed from the ferromagnetic to the paramagnetic phase.

4. Conclusion

In this study, we have investigated the thermodynamic and magnetic properties of GaMnAs cylindrical nanoshells under Rashba spin-orbit interaction. Our results reveal that RSO coupling significantly modifies energy levels, heat capacity, entropy, and magnetic susceptibility. Notably, the system exhibits a low-temperature Schottky anomaly in heat capacity and a field- and temperature-driven transition from ferromagnetic to paramagnetic behavior. These results not only deepen our understanding of spin-orbit-coupled nanostructures but also have important application implications. The tunability of magnetic phase and entropy via external fields suggests potential use in spintronic memory and switching devices, quantum phase-change components, and nanoscale thermal sensors. Additionally, the interplay of geometry and spin interaction in such curved systems could be harnessed in curvature-sensitive spin filters or thermoelectric nanodevices. We anticipate that our findings will inspire future experimental and theoretical efforts aimed at developing functional materials based on spin-orbit-modulated thermodynamic properties.

Acknowledgments

LMP and DL acknowledge financial support from Centers of Excellence with BASAL/ANID financing, CIA250002, CEDENNA and FONDECYT 1241985. LMP, PD and DL acknowledge partial financial support from FONDECYT 1231020.

Conflicts of interest

The authors declare that there is no conflict of interest regarding the publication of this manuscript.

Data availability statement

No new data were created or analysed in this study.

Contributions

All the authors contributed equally to the manuscript.

References

[1] Hirohata A, Yamada K, Nakatani Y, Prejbeanu I-L, Diény B, Pirro P and Hillebrands B 2020 Review on spintronics: Principles and device applications *J. Magn. Magn. Mater.* **509** 166711
[2] Sarma S D 2001 Spintronics: A new class of device based on electron spin, rather than on charge, may yield the next generation of microelectronics *Am. Sci.* **89** 516–23
[3] Raju R, Rao K V, Waghmare U and Rout C 2008 Honeywell technology solutions, bangalore; jncasr, bangalore; stockholm university, sweden *Unpublished Work or Presentation* Presented on 22nd February 2008
[4] Flatté M E 2009 Silicon spintronics warms up *Nature* **462** 419–20
[5] Rashba E I 1960 Spin-orbit coupling in condensed matter physics *Sov Phys Solid State* **2** 1109
[6] Dresselhaus G 1955 Spin-orbit coupling effects in zinc blende structures *Phys. Rev.* **100** 580–6
[7] De Groote J-J S, Hornos J E M and Chaplik A V 1992 Thermodynamic properties of quantum dots in a magnetic field *Phys. Rev. B* **46** 12773–6
[8] Hassanabadi H, Rahimov H and Zarrinkamar S 2011 Rashba coupling in three-electron-quantum dot under cylindrical symmetry: An exact solution *Ann. Phys., NY* **326** 2957–62
[9] Hassanabadi H, Rahimov H and Zarrinkamar S 2012 Analytical treatment of a three-electron-quantum dot under rashba spin-orbit interaction *Few-Body Syst.* **52** 87–95
[10] Zhang L and Wang J 2011 Spin transport in a rashba ring-quantum dot system pumped by microwave fields *Commun. Theor. Phys.* **55** 709
[11] Jin-Liang L and Yu-Xian L 2010 Spin current through triple quantum dot in the presence of rashba spin-orbit interaction *Chin. Phys. Lett.* **27** 057202
[12] Kushwaha M S 2008 Magneto-optics of single rashba spintronic quantum dots subjected to a perpendicular magnetic field: Fundamentals *J. Appl. Phys.* **104** 083714
[13] Gumber S, Kumar M, Gambhir M, Mohan M and Jha P K 2015 Thermal and magnetic properties of cylindrical quantum dot with asymmetric confinement *Can. J. Phys.* **93** 1264–8
[14] Boyacioglu B and Chatterjee A 2012 Heat capacity and entropy of a gaas quantum dot with gaussian confinement *J. Appl. Phys.* **112** 083514
[15] Nguyen N T T and Peeters F M 2008 Magnetic field dependence of the many-electron states in a magnetic quantum dot: The ferromagnetic-antiferromagnetic transition *Phys. Rev. B* **78** 045321
[16] Shi K-L and Jiang W 2025 Dynamic magnetic behaviors and magnetocaloric effect of CrI_3-like bilayer structure *Phys. Scr.* **100** 035908
[17] Shi K-L, Jiang W and Wu W-C 2024 Dynamic magnetic and magnetocaloric behaviors of a Kagome-like cluster *Physica A* **651** 130003

[18] Shi K-L, Si N and Jiang W 2024 Dynamic magnetic properties and magnetocaloric effect of a decorated square structure *Chin. J. Phys.* **92** 1395–413
[19] El-Yadri M, Hamdaoui J E, Aghoutane N, Pérez L M, Baskoutas S, Laroze D, Díaz P and Feddi E M 2023 Optoelectronic properties of a cylindrical core/shell nanowire: Effect of quantum confinement and magnetic field *Nanomaterials* **13** 1334
[20] Kria M, Feddi K, Aghoutane N, El-Yadri M, Pérez L, Laroze D, Dujardin F and Feddi E 2020 Thermodynamic properties of SnO_2/GaAs core/shell nanofiber *Physica A* **560** 125104
[21] Khordad R 2018 Simultaneous effects of electron-electron interactions, rashba spin-orbit interaction and magnetic field on susceptibility of quantum dots *J. Magn. Magn. Mater.* **449** 510–4
[22] COMSOL Multiphysics® 2015 Reference Manual, Version 5.2, COMSOL AB, Stockholm, Sweden (https://comsol.com/release/5.2)
[23] Huang K 2009 *Introduction to Statistical Physics* (Chapman and Hall/CRC)
[24] Askerov B M and Figarova S R 2010 Quantum statistics: equilibrium electron gas *Thermodynamics, Gibbs Method and Statistical Physics of Electron Gases* (Springer) pp 213–96
[25] Shannon C E 1948 A mathematical theory of communication *The Bell System Technical Journal* **27** 379–423
[26] Tsallis C 1988 Possible generalization of boltzmann-gibbs statistics *J. Stat. Phys.* **52** 479–87
[27] Chen L, Yang X, Yang F, Zhao J, Misuraca J, Xiong P and von Molnár S 2011 Enhancing the curie temperature of ferromagnetic semiconductor (ga,mn)as to 200 k via nanostructure engineering *Nano Lett.* **11** 2584–9
[28] Lang R, Winter A, Pascher H, Krenn H, Liu X and Furdyna J K 2005 Polar kerr effect studies of $ga_{1-x}mn_xAs$ epitaxial films *Phys. Rev. B* **72** 024430
[29] Feddi E, El-Yadri M, Dujardin F, Restrepo R L and Duque C A 2017 Photoionization cross section and binding energy of single dopant in hollow cylindrical core/shell quantum dot *J. Appl. Phys.* **121** 064303
[30] Voskoboynikov O, Bauga O, Lee C P and Tretyak O 2003 Magnetic properties of parabolic quantum dots in the presence of the spin–orbit interaction, *J. Appl. Phys.* **94** 5891–5
[31] Wagner M, Merkt U and Chaplik A V 1992 Spin-singlet-spin-triplet oscillations in quantum dots *Phys. Rev. B* **45** 1951–4